



# Ablation of a Solid Material by High Temperature Liquid Jet Impingement: An Application to Corium Jet Impingement on a Sfr Core-Catcher

Alexandre Lecoanet, Michel Gradeck, Xiaoyang Gaus-Liu, Thomas Cron, Beatrix Fluhrer, Frédéric Payot, Christophe Journeau, Nicolas Rimbart

## ► To cite this version:

Alexandre Lecoanet, Michel Gradeck, Xiaoyang Gaus-Liu, Thomas Cron, Beatrix Fluhrer, et al.. Ablation of a Solid Material by High Temperature Liquid Jet Impingement: An Application to Corium Jet Impingement on a Sfr Core-Catcher. Journal of Nuclear Engineering and Radiation Science, 2022, 8 (1), pp.11308. 10.1115/1.4051448 . hal-03312388

**HAL Id: hal-03312388**

**<https://hal.univ-lorraine.fr/hal-03312388>**

Submitted on 26 Jan 2024

**HAL** is a multi-disciplinary open access archive for the deposit and dissemination of scientific research documents, whether they are published or not. The documents may come from teaching and research institutions in France or abroad, or from public or private research centers.

L'archive ouverte pluridisciplinaire **HAL**, est destinée au dépôt et à la diffusion de documents scientifiques de niveau recherche, publiés ou non, émanant des établissements d'enseignement et de recherche français ou étrangers, des laboratoires publics ou privés.



Distributed under a Creative Commons Attribution 4.0 International License

# **Ablation of a solid material by high temperature liquid jet impingement: an application to corium jet impingement on a SFR core-catcher**

**Alexandre Lecoanet**

CEA, DES/IRENE/DTN/SMTA/LEAG, Cadarache, 13108 Saint-Paul-lez-Durance – FRANCE  
alexandre.lecoanet@univ-lorraine.fr

**Michel Gradeck<sup>1</sup>**

Université de Lorraine, CNRS, LEMTA, F-54000 Nancy, France  
LEMTA 2 avenue de la forêt de Haye BP90961 54505 Vandoeuvre les Nancy Cedex  
michel.gradeck@univ-lorraine.fr

**Xiaoyang Gaus-Liu**

Karlsruhe Institute of Technology (KIT)  
Hermann-von-Helmholtz-Platz 1, 76344, Eggenstein-Leopoldshafen, Germany  
Xiaoyang.gaus-liu@kit.edu

**Thomas Cron**

Karlsruhe Institute of Technology (KIT)  
Hermann-von-Helmholtz-Platz 1, 76344, Eggenstein-Leopoldshafen, Germany  
Thomas.cron@kit.edu

**Beatrix Fluhrer**

Karlsruhe Institute of Technology (KIT)  
Hermann-von-Helmholtz-Platz 1, 76344, Eggenstein-Leopoldshafen, Germany  
Beatrix.fluhrer@kit.edu

**Frédéric Payot**

Commissariat à l'Energie Atomique et aux Energies Alternatives  
CEA, DES/IRENE/DER, Cadarache, 13108 Saint-Paul-lez-Durance – FRANCE  
frederic.payot@cea.fr

**Christophe Journeau**

CEA, DES/IRENE/DTN/SMTA/LEAG, Cadarache, 13108 Saint-Paul-lez-Durance – FRANCE  
christophe.journeau@cea.fr

---

<sup>1</sup> Full professor at Université de Lorraine - FRANCE.

**Nicolas Rimbert**

Université de Lorraine, CNRS, LEMTA, F-54000 Nancy, France

LEMETA 2 avenue de la forêt de Haye BP90961 54505 Vandoeuvre les Nancy Cedex

Nicolas.rimbert@univ-lorraine.fr

**ABSTRACT**

*This paper deals with ablation of a solid by a high temperature liquid jet. This phenomenon is a key issue to maintain the vessel integrity during the course of a nuclear reactor severe accident with melting of the core. Depending on the course of such an accident, high temperature corium jets might impinge and ablate the vessel material leading to its potential failure. Since Fukushima Daiichi accident, this severe accident scenario draws more concern in the nuclear safety policy and new mitigation measures are under study. As a designed safety feature of a future European Sodium Fast Reactor (SFR), bearing the purpose of quickly draining of the corium out of the core and protecting the reactor vessel against the attack of molten melt, the in-core corium is relocated via discharge tubes to an in-vessel core-catcher has been planned. The core-catcher design to withstand corium jet impingement demands the knowledge of very complex phenomena such as the dynamics of cavity formation and associated heat transfers. Even studied in the past, no complete data are available concerning the variation of jet parameters and solid structure materials. For a deep understanding of this phenomenon, new tests have been performed using both simulant and prototypical jet and core catcher materials. Part of these tests have been done at University of Lorraine (UL) using hot liquid water impinging on transparent ice block allowing for the visualizations of the cavity formation. Other tests have been performed in Karlsruhe Institute of Technology (KIT) using liquid steel impinging on steel block.*

## INTRODUCTION

The Fukushima accident tragically demonstrated that the meltdown of a nuclear plant reactor core is possible and the severe accident measures should be examined, which is also a topic of SFR design. There are several situations that can lead to core meltdown in SFR. The starting point of this study is the situation where part of the SFR core has already melted. Consequently, safety standards and severe accident management have been updated for future nuclear plants as well as all existing ones. The safety strategy considering an in-vessel confinement needs several prevention and mitigation devices.

Regarding the severe accident mitigation, the European requirements rely on a safety design to control the molten fuel relocation in sub-critical and coolable configurations. For this reason, it has recommended two important mitigation concepts in the new European sodium fast neutron reactor (ESFR):

- Corium in-core transfer tubes to carry the molten fuel away from the core region, thus reducing the risk of prompt criticality and mechanical loading. These channels are located in the core in the form of empty fuel sub-assemblies, filled with sodium. These sub-assemblies are extended below the core by tubes which pass through the diagrid/strongback leading into lower head in order to channel the molten fuel towards the core catcher at the bottom of the reactor vessel.
- A core catcher in the vessel lower head to collect the corium and remove its decay heat. The design of the core catcher and its protective coating are under study. It is worth noting that the core catcher coating materials could be a metallic material.

In the severe accident situation, the molten fuel and structure stainless steel material lead to a complex mixture with a very high melting point ( $>2000\text{ }^{\circ}\text{C}$ ) which is named corium. So, under certain conditions, the corium can be composed of mainly two phases. An oxide phase coming from the melting of nuclear fuel and a metallic phase coming from the melting of in-vessel structure elements. In case of melting, the corium

oxide could flow within numerous fusible discharge tubes toward the core catcher and be spread in it, where it will be cooled down and gradually solidified by the surrounding liquid sodium coolant (Fig. 1). But due to the high difference between the initial temperature of the corium jet and the melting temperature of the coating material of the core-catcher, the corium jets would ablate the core-catcher. Note that the ablation will also depend on corium composition. In case of a metallic coating material, the ablation could be more dramatic if a coherent metallic jet firstly reaches in the core-catcher in comparison to oxide corium, since oxide corium can form a solid crust layer due to its high melting temperature. In order to reduce uncertainties regarding the failure of the core catcher, knowledge of the heat transfer rates in this particular situation needs more studies. Experimental data are thus needed to simulate the ablation behavior of long duration jets impinging a thick sacrificial material plate. In this scope, experimental tests with simulants have been carried out by using conditions which are representatives (e.g. Reynolds and Prandtl numbers) for ESFR severe accident conditions.

For that purpose, in the framework of the ESFR SMART project launched in 2017, The energy & theoretical and applied mechanics laboratory (LEMTA) of University of Lorraine (France) and KIT (Germany) have performed different complementary tests to understand more deeply the ablation phenomena and to bring useful data for the design of the core-catcher. Experimental tests performed in LEMTA used simulant materials, namely hot water jet / transparent ice and KIT used the molten stainless steel / stainless steel prototypic system. The LEMTA's tests are useful to visualize the whole ablation process taking the advantage of the transparency of the ice while KIT experiments are closer to the target case with prototypical conditions. The complementary approaches of both experimental facilities can provide useful information about the process of ablation. In what follows, a short literature review about jet impingement heat transfer with phase change is provided. Indeed, some few studies with melting of the solid are available; they provided some scaling laws for heat transfer. Then, we describe the details of each test bench and experiments carried out

at LEMTA (i.e HAnSoLO<sup>2</sup> experiments) and at KIT (i.e JIMEC<sup>3</sup> experiments). Finally, the experiments are analyzed and the main findings will be highlighted.

## JET IMPINGEMENT HEAT TRANSFER WITH PHASE CHANGE

Several different situations can be considered of the jet on the way to the core catcher with the surrounding liquid sodium as coolant. i) Breakup of the jet and spreading of debris in the core catcher; (ii) Vaporization of Na with its vapor flowing upwards very dynamically, even explodes, and thus prevents the downward flow of coherent corium jet, (iii) a coherent jet of corium impinging directly onto the core-catcher. The last situation is here considered as the most unfavorable for core catcher plate integrity and thus is considered for the design of the core-catcher. In this last case, the first step of the ablation process can be simply described as shown in Fig. 2. When both the jet and the solid wall are of similar composition (water/ice, metal/metal or oxide/oxide), the energy which is brought by the jet heats the solid wall and can melt it (Case 1, Fig. 2). If the wall is metallic and the jet is composed of oxide, a crust can form [1] due to the high oxide solidification temperature (Case 2, Fig. 2). The crust thermal resistance would decrease the heat flow but melting could still occur beneath it. Crust's stability is something very difficult to fully model as it depends mainly on its thermal [2] and mechanical properties [3]. A third case (not described in Fig. 2) is the initial solidification of liquid from the jet without melting of the solid wall and thereafter meltdown; this situation can happen if the initial contact temperature is lower than the melting point of the jet material. The contact temperature is determined by the initial temperature of two contact media and their thermal inertia and is provided by Eq. 1, coming from the exact solution heat transfer between two infinite media put together in contact at  $t=0$ .

---

<sup>2</sup> Hot Ablation of a Solid by a liquid jet - Observations

<sup>3</sup> Jet Impingement on Metallic Core catcher

$$T_{contact} = T_{0,S} + \frac{T_J - T_{0,S}}{1 + \sqrt{\frac{\rho_S c_{p,S} k_S}{\rho_J c_{p,J} k_J}}} \quad (1)$$

The lifetime of the solidified layer (i.e. the crust) was estimated to be low by Sato et al. [4], see Eq. 2:

$$t_{life} \sim \frac{\pi k_S^2 (T_{m,S} - T_{0,S})^2}{4 \alpha_S q^2} \quad (2)$$

and thus it is negligible in this study. The most dynamic ablation process occurs in the Case I, and is the topic of this study.

Experiments to characterize the ablation of a solid by a liquid jet have already been carried out in the past [4,5] with different couples of simulant materials, e.g Tin/Tin and Stainless steel / stainless steel for [4], NaCl/Tin and Al<sub>2</sub>O<sub>3</sub>/Steel for [5], water/ice for [6]. For these experiments, an induction heating device was used to achieve melting of alumina (Al<sub>2</sub>O<sub>3</sub>) or salt (2054 °C and 800 °C) which is then poured as a jet onto tin or steel walls. The governing parameters in these tests are the volume flow rate of the jet, its velocity and temperature, the temperature of the solid interface, the duration of the jet, the distance between the nozzle and the solid interface, the angle of inclination of the plate, the nature of the jet and of the solid and therefore their thermodynamic, thermal and dynamic properties.

These authors have particularly shown that in a first step, the ablation rate is quite constant and when the depth of the cavity formed exceeds 3 to 4 times the diameter of the jet, a change in the flow dynamics can occur and consecutively the ablation rate can decrease sharply. This change is due to a transition of the hydrodynamics known as the "pool effect" phenomenon. In this situation, a liquid pool forms in the cavity which reduces the flow of heat to the wall.

What we learnt from these publications is that the shape of the cavity is depending on many parameters among which are surely, jet initial conditions, stability of the jet and the liquid film and thus, it is very important to understand which parameters play the first order of role.

To go deeply in the understanding of ablation phenomena, physics has to be analyzed more. This has been first done in two complementary papers which are the works of Swedish et al. [7] based on the problem defined by Roberts [8]. The study of Swedish et al. [7] considered the impact of a laminar jet on a thin layer of liquid resulting from the melting of the solid wall. Considering the classical equations of momentum, energy and continuity for the jet and the ablated layer, the problem is assumed stationary and the thickness of the melted layer, constant; this melted layer, also considered immiscible with the jet, is an additional thermal resistance between the jet and the solid wall.

When a turbulent liquid jet impinges a solid wall, flow laminarization is likely to occur [9]. Therefore, the approach of Swedish et al. [7] is still valid as long as the jet is not interacting with a pool (i.e. no pool effect is considered). It can be taken as a basis for the heat transfer analysis as long as pool effect has not yet occurred.

The melting velocity is thus one of the most important parameter to estimate as it is directly linked to the heat transfer coefficient, assuming it can be expressed by a Newton's law. The analysis of the set of equation describing the melting phenomena gives the following relationship for the heat transfer coefficient, Sato et al. [4]:

$$h_{exp} = \frac{V_m \rho_S [L_S + C_{p,S}(T_{m,S} - T_{0,S})]}{(T_J - T_{m,S})} \quad (3)$$



From Eq (3), we can estimate the experimental Nusselt number (Eq. 4a) and then, making a regression on the experimental points, the scaling law linking the Nusselt number to the Reynolds and Prandtl number can be established, as generally described in Eq. (4b).

$$Nu_{exp} = \frac{h_{exp} D_J}{k_J} = C_{te} Re^a Pr^b \quad (4a)$$

$$Nu = C_{te} Re^a Pr^b \quad (4b)$$

As we can see, the initial temperature of the solid wall is a key parameter and thus must be measured. The velocity of the jet is taken at the impact; so, the acceleration of the jet during its fall must be accounted as it modifies its diameter. Finally, without surprise, the temperature of the jet must be also known accurately as it is the jet that brings the heat necessary to melt the solid wall. This melting process depends also on the thermal property of the solid wall, hence its ability to diffuse the heat far from the melting front.

As it can be seen, this is a very complex and intricate phenomenon which depends on many parameters as outside flow (i.e. flow regime), heat dissipation within the wall, melting of the wall (Fig. 3), and also possibility of a crust formation and its stability.

## EXPERIMENTAL SET-UP

### HAnSoLO experiments at LEMTA

The HAnSoLO experimental setup has been designed during the PhD thesis of Alexandre Lecoanet [10] with the purpose of providing usable visualizations of the cavity formation during the interaction of a hot liquid water jet and a solid body (i.e. transparent ice block), to test a wide range of Reynolds number (for different jet nozzle diameter) and different initial liquid jet temperature, as can be seen in the following table 1.

Ablation front lower position is recorded using a high-speed camera. To the best of author's knowledge, it is the first time that the entire ablation process was recorded in real time for a downward flowing jet. It thus makes it possible to estimate the ablation velocity during the process. Another important point provided by this experimental approach is the ability to catch accurately the time point of the transition to pool-effect.

A steady jet at fixed flowrate and controlled temperature were ensured. Water was heated in a tank (Fig. 4), flow rate of jet was delivered by an eccentric screw pump and measured by an electromagnetic flowmeter. A three-way valve located before the nozzle to keep the water in a loop (back to the tank) until a stable temperature was reached. The valve was commuted at test beginning.

As fall height/ jet diameter ratio,  $H/D_j$ , can influence ablation in many ways: (i) jet velocity change by gravity acceleration; (ii) the velocity profile of the jet cross section is not uniform at the outlet and relaxes toward an almost uniform velocity profile [11] if  $H/D_j$  is greater than 6 [2, 9] (so, we ensure a minimum height of  $6D$  but at least  $<10D$  in order for the jet to be not disturbed by the surrounding air). Nozzle's length is 50 times of its inner diameter to ensure a fully developed turbulent flow at its outlet. Even if the temperature of the jet is measured, a controlled heating liner is coiled around it to bring it to prescribed temperature and to reduce heat losses. Ice block is maintained by means of rods inserted inside (cf. Fig. 5), which are later screwed onto a positioning apparatus. Two thermocouples are also embedded to control the ice temperature.

### **JIMEC test facility at KIT**

KIT has a long history on the generation of corium simulant by thermite reaction and on the investigation of the erosion on concrete substrate by corium. In KAJET<sup>4</sup> experiment for example, the erosions on the concrete substrate by metallic jet and by

---

<sup>4</sup> Karlsruhe Jet Experiment

oxide jet were studied [12]. The erosion of a metallic substrate in the JIMEC experiment is a new challenge, since different as the instrumentation in the concrete, the montage of the thermocouple inside the metallic substrate requires special design and technique. Also, the amount of the metallic mass and its composition analog to stainless steel requires rich knowhow on the thermite reaction variations.

The JIMEC test facility includes a thermite reaction crucible, a pouring spout for redirection of oxide melt after the outflow of the metallic melt, an oxide melt collector and the test substrate, see Fig. 6 (schematics of JIMEC facility) and Fig. 7 (JIMEC-2 test set-up). The falling height from the crucible outlet to the substrate is 1.08 m and 0.94 m in JIMEC-1 and JIMEC-2 test respectively. The thermite reaction crucible can contain 3 tons of thermite material. It has a steel shell and 80 mm magnesia refractory liner inside. The outflow opening at the bottom is 40 mm in diameter for JIMEC-1 and 30 mm in diameter for JIMEC-2. After ignition, the thermite reaction is usually completed within 30 to 60 s. In the crucible, the metallic part of the melt segregates beneath the oxidic part of the melt due to its higher density. A thermocouple above the outflow opening detects the end of the thermite reaction. Based upon this thermocouple signal, the opening mechanism is immediately manually activated and the outflow of the melt starts. At first, the metallic melt flows out as a melt jet, followed by the oxide melt.

The pouring spout for the redirection of the oxide melt responds upon a manual signal right after the outflow of the metallic melt, and can be driven from the rear side to the center area beneath the crucible. The refractory lining in the crucible and in the pouring spout are preheated to prevent melt solidification at these locations.

### **Simulant and prototypical materials for the impacted substrates**

For HAnSoLO experiment, the test substrate is transparent ice. To produce transparent ice block, a mold is initially filled with softened water; then, the mold is cooled from the bottom part of it while its other sides are kept adiabatic ensuring a 1D cooling. Additionally, a slight flow of the water to be freeze is necessary to remove the

dissolved gas from the ice. By doing that, it is possible to obtain transparent block (Fig. 5). In Fig. 5, the ice block is in upside down position and we can observe grey bars (in fact four) which are frozen in the ice and serve as holding device. Two thermocouples embedded in the ice (green cable) measure the temperature of the block of ice with a precision of 2 °C. Once the ice block is ready for the test, it is placed on a support device which can be tilted to test the impact of different impingement angle. But this parameter has not been considered in this paper. The dimension of the ice block is about 25 x 25 x 50 cm<sup>3</sup>. Position of the ablation front is recorded with a high-speed camera. A home-made Python program is used for the post-processing of the film and allows for the estimation of ablation rate.

For JIMEC's tests, the substrate is a cylindrical stainless steel block with 416 mm in height and 425 mm in diameter. The material of the substrate is X5 Cr Ni 18 10, (German 1.4301, US 304) with a melting temperature of 1450 °C. To detect the ablation process and substratum temperature, 41 K-type thermocouples in stainless steel sheaths (up to 1370 °C) were first inserted within an "Instrumentation plate" which was implemented inside the substrate at one-half of the substrate vertical cross-section, see Fig. 8. These thermocouples are used to detect the melting front as well as to follow the formation of the cavity as a function of time.

The metallic melt is generated by thermite reaction to produce 1000 kg of molten metal analogous to stainless steel 1.4301 (X 5 Cr Ni 18 10) and therefore analogous to the substrate material. The composition of stainless steel 1.4301 according to DIN EN 10088-3 is given in Table 2.

About 2000 kg of different components (commercial thermite, chromium oxide, aluminium, nickel and calcia) have been used to produce 1000 kg of the metallic melt with designed composition and temperature. After the tests, the ablated substrate was cut through the axial center. Several samples of the metal melt were taken to determine

the jet and substrate metal composition. The material properties of the metallic melt and the test substrate are given in Table 3.

Details of the experimental test runs made at LEMTA and KIT can be found in tables 4 and 5.

Regarding the uncertainties on measurements performed with HAnSoLO, detailed informations about them can be found in the PhD thesis document of Lecoanet [10]. We also provide these informations in the table 4b.

## EXPERIMENTAL RESULTS

JIMEC-1 and JIMEC-2 provided very high Reynolds numbers, respectively  $Re = 5.82 \cdot 10^5$  and  $Re = 4.2 \cdot 10^5$  with a Prandtl number less than 1 (0.05) which could be encountered in a SFR. HAnSoLO's experiments have been performed at lower Reynolds numbers ( $Re < 150\,000$ ) but higher Prandtl number ( $Pr > 2.5$ ); this last parameter could be responsible for different behavior as Prandtl number gives an idea of the relative importance of thermal and dynamic boundary layers. A high Prandtl number indicates that the temperature profile in the fluid will be strongly influenced by the velocity profile.

The visualizations performed with HAnSoLO have clearly highlighted the two expected regimes, namely the film flowing regime for which the jet spread on a concave surface and the pool regime for which the jet interacts with a pool of liquid (Fig. 9). Note that the first regime can be also observed for the JIMECs experiments as the spread of impinging onto the embryo of formed cavity forms some splashing while in the pool regime, no such atomization can be observed (Fig. 10). The time of transition between the two ablation regimes can thus be estimated visually for HAnSoLO and JIMEC but can also be estimated through a change in the melting velocity; this time is noted  $t_{pe}$ . In the case of JIMEC tests, this time was estimated to 18-19 s for JIMEC-1 and 15 s for JIMEC-2

with a constant melting velocity about 17-18 mm/s before decreasing to 7-8 mm/s in the pool regime.

HAnSoLO experimental runs (see Table 4a) performed at LEMTA have been post-processed and the first results are the depth of the formed cavity as a function of time. These results coming from different experiments have been normalized to be compared. Firstly the time is normalized considering the time  $t_{pe}$  (i.e. time of transition to pool regime), the melting velocity  $V_m$  and the diameter of the jet  $D_j$ , as described in Eq (5) , while the depth of the cavity is also normalized as the description in Eq. (6).

$$t^* = \frac{(t-t_{pe})V_m}{D_j} \quad (5)$$

$$Z^* = \frac{(Z-Z_{pe})V_m}{D_j} \quad (6)$$

From the Fig. 11, it can be observed that the melting velocity is constant before the pool regime as any curves is aligned on the bisector. As the transition occurs ( $t^*=0$ ), a deviation from the bisector is not observed immediately for the HAnSoLO experiments which continue to follow the bisector until  $t^*=2$  and deviate from it and behave differently for  $t^*>5$ . That is something which must be clarified but from a thermal point of view, it shows that even the dynamics is very different from the film flowing regime to the pool regime, the heat transfer is not immediately modified. In HAnSoLO experiments an increase in ablation velocity is witnessed for several experiments. For the JIMEC tests, post mortem cuts of the test substrates have been performed and we obtained the contour of the cavities, Fig. 12. A hole can be observed on the side of the test substrate corresponding to JIMEC1 test (Fig. 12a). It explains why the test substrate has not been completely pierced contrary to the case of JIMEC2 (Fig. 12b). Nevertheless, the shape of both cavities is similar even obtained for different Reynolds number of the jet.

## HEAT TRANSFER ANALYSIS

From the estimation of the melting velocities obtained after some post-processing, Nusselt numbers for HAnSoLO experiments have been calculated before the pool effect regime thanks to equations (3) and (4). Then, they have been compared with available scaling laws from different works. Nusselt numbers calculated from the method proposed by Furutani et al [5] or by the correction of the scaling law proposed by Sitharamaya et al [15] are lower than the experimental results, but remain of the same order of magnitude. It is then possible to determine a confidence interval for Nusselt number using respectively the approach of Furutani et al. [5] and that of Sato et al [4]. This assumption is consistent with the fact that using [5], Nusselt numbers are underestimated for HAnSoLO results obtained with the highest Reynolds numbers. This is shown in Fig. 13. Also, we can see in Fig. 12 that the correlation of Sato et al [4] and of Saito et al. [1] do not fit HAnSoLO data. This may be due to the difference in the Prandtl number domain between HAnSoLO experiments and these studies and also to the fact that a crust is formed during the experiments of Saito et al. [1]. But, Nusselt numbers from HAnSoLO fit quite well with the scaling laws of Furutani et al. [5] and Sitharamayya et al. [15].

These comparisons show that the results obtained with simulant materials (i.e. Ice/water) are very consistent. Nusselt numbers terms are unfortunately not yet available from JIMEC's experiments.

## **CONCLUDING REMARKS**

This experimental work has provided some relevant results for the design of the core-catcher, a mitigation device located in the lower part of the vessel of the future European SFR. Two different experimental benches have been used, JIMEC has been developed at KIT to perform steel/steel experiments while HAnSoLO has been built at UL to perform experiments using liquid water/ice as simulant materials. The first one, although operating only two experiments, gives relevant post mortem results and

confirms the two regimes yet observed by previous authors. The first regime is a film flowing regime, recognizable by the splashing of the jet, with a very effective heat transfer. The second one, known as a pool regime, although less effective does not stop the crater formation. HAnSoLO allows for the whole process real time analysis as it uses transparent ice as solid simulant.

The two JIMEC experiments carried out at KIT used a jet of molten steel which impinged directly on a steel block of same composition. The two tests which differ in the Reynolds number (diameter and velocity) and Prandtl number need further analysis to get properly the heat transfer coefficient associated to the melting velocities. Nevertheless, valuable results have been obtained from these prototypical tests as the shape of the cavities. Using HAnSoLO tests, we were able to analyze the dynamics of the cavity formation and provide valuable results for heat transfer. We show that the estimated Nusselt number compares well with existing scaling laws [5,15]. More analysis about heat transfer in the film regime can be found in [16].

The future work will be dedicated to the modelling of the cavity formation. Analytical models are under study as well as some numerical modelling using a multiphase CFD code currently developed at CEA.

## **ACKNOWLEDGMENT**

We, Prof. Nicolas Rimbert and Prof. Michel Gradeck, are grateful to Jean-Yves Morel, Head of the “technical” department of LEMTA; he perfectly managed the design and the building of the HAnSoLO set-up with the help of Jeremy Bianchin, Sebastien Lejeune, Franck Demeurie, Eric Blaise, Christophe Gigant. We are also thankful to Mathieu Weber, Head of “Electronics, Metrology and Instrumentation” Department who performed the instrumentation of the experiment with the help of Ing. Hadrien Chaynes, Jamal Ouahajjou and Ing. Simon Weber.



## **FUNDING**



The research leading to these results has received funding from the Euratom research and training program 2014-2018 under grant agreement No 754501

## NOMENCLATURE

$a, b, C_{te}$	constant
$C_{p,J}$	Specific heat capacity of the liquid jet, J/kg K
$C_{p,S}$	Specific heat capacity of the solid, J/kg K
$D_J$	Diameter of the jet, m
$h_{exp}$	Estimated heat transfer coefficient, W/m <sup>2</sup> K
$k_J$	Conductivity of the liquid jet, W/m K
$k_S$	Conductivity of the solid, W/m K
$L_S$	Latent heat of the solid, J/kg
$q$	Heat flux, W/m <sup>2</sup>
$t$	Time, s
$t_{pe}$	Time corresponding to ablation regime transition to pool effect, s
$t_{life}$	Life time of the hypothetical crust, s
$T_{contact}$	Initial contact temperature, K
$T_{0,S}$	Initial solid temperature, K
$T_{m,S}$	melting temperature of the solid, K
$T_J$	jet temperature, K
$V_m$	Melting velocity, m/s
$z$	Depth of the cavity, m

$Z_{pe}$  Depth of the cavity at the transition to pool effect, m

### Greek letter

$\alpha_s$  heat diffusivity of the solid, m<sup>2</sup>/s

$\mu$  Dynamic viscosity of the liquid, kg/m s

$\rho$  Density, kg/m<sup>3</sup>

### Non-Dimensional Number

B Melting number,  $\frac{c_{p,J}(T_J - T_{m,S})}{L_S + c_{p,S}(T_{m,S} - T_{0,S})}$

Nu Nusselt number,  $\frac{h.D}{k}$

Pr Prandtl number,  $\frac{\mu c_{p,J}}{k_J}$

Re Reynolds number,  $\frac{\rho_J V_J D_J}{\mu_J}$

$t^*$  Dimensionless ablation time period before pool effect transition

$Z^*$  Dimensionless ablation depth before pool effect transition

### Subscripts or Superscripts

\*

 design a dimensionless parameter

0 Initial

*calc* Estimated with a scaling law

<i>contact</i>	Contact temperature
<i>exp</i>	experimental
<i>J</i>	jet
<i>life</i>	Life time
<i>m</i>	Melting
<i>pe</i>	At pool effect transition
<i>S</i>	solid

#### Acronyms

<i>ESFR</i>	European Sodium Fast Reactor
<i>LEMTA</i>	Laboratoire Energies & Mécanique Théorique et Appliquée
<i>KIT</i>	Karlsruhe Institut of Technology
<i>ESFR SMART</i>	
<i>HAnSoLO</i>	Hot Ablation of a Solid by a Liquid jet - Observations
<i>JIMEC</i>	Jet Impingement on Metallic Core catcher
<i>UL</i>	University of Lorraine
<i>CFD</i>	Computational Fluid Dynamics
<i>CEA</i>	Commissariat à l’Energie Atomique et aux Energies Alternatives
<i>KAJET</i>	Karlsruhe Jet Experiments



## REFERENCES

- [1] M. Saito, K. Sato, A. Furutani, M. Isozaki, S. Imahori, Y. Hattori, Melting attack of solid plates by a high temperature liquid jet — effect of crust formation, Nuclear Engineering and Design 121 (1) (1990) 11 – 23, [https://doi.org/10.1016/0029-5493\(90\)90003-G](https://doi.org/10.1016/0029-5493(90)90003-G).
- [2] M. Epstein, M. J. Swedish, J. H. Linehan, G. A. Lambert, G. M. Hauser, L. J. Stachyra, Simultaneous melting and freezing in the impingement region of a liquid jet, AIChE J 26 (5) (1980) 743–751, <https://doi:10.1002/aic.690260507>
- [3] D. A. Powers, Erosion of steel structures by high-temperature melts, Nuclear Science and Engineering 88 (3) (1984) 357–366, <https://doi:10.13182/NSE84-A18589>
- [4] K. Sato, A. Furutani, M. Saito, M. Isozaki, K. Suganuma, S. Imahori, Melting attack of solid plates by a high-temperature liquid jet [ii] — erosion behavior by a molten metal jet, Nuclear Engineering and Design 132 (2) (1991) 171 – 186. [doi.org/10.1016/0029-5493\(91\)90264-I](https://doi.org/10.1016/0029-5493(91)90264-I)
- [5] A. Furutani, S. Imahori, K. Sato, M. Saito, Erosion behavior of a solid plate by a liquid jet – effect of molten layer, Nuclear Engineering and Design, Volume, 132, 1991, Pages 153-169. [https://doi.org/10.1016/0029-5493\(91\)90263-H](https://doi.org/10.1016/0029-5493(91)90263-H)
- [6] R. R. Gilpin, The Ablation of Ice by a Water Jet, Transactions of the Canadian Society for Mechanical Engineering, vol. 2, pp. 91–96, June 1973. <https://doi.org/10.1139/tcsme-1973-0014>
- [7] M. Swedish, M. Epstein, and John H. Linehan et al. Surface ablation in the impingement region of a liquid jet, AIChE Journal, Vol. 25, 630–638, 1979. <https://doi.org/10.1002/aic.690250409>
- [8] L. Roberts, On the melting of a semi-infinite body of ice placed in a hot stream of air, Journal of Fluid Mechanics, Vol. 4, 1958, pp 505-528. <https://doi.org/10.1017/S002211205800063X>
- [9] A. Y. Tong, A numerical study on the hydrodynamics and heat transfer of a circular liquid jet impinging onto a substrate, Numerical Heat Transfer, Part A: Applications 44 (1) (2003) 1–19, <https://doi.org/10.1080/713838171>
- [10] A. Lecoanet, Etude de l’ablation d’une paroi solide par un jet liquide, thèse Université de Lorraine, janvier 2021. <http://www.theses.fr/2021LORR0015>
- [11] A. Bin, Minimum air entrainment velocity of vertical plunging liquid jets, Chemical Engineering Science 43 (2) (1988) 379 – 389, [https://doi.org/10.1016/0009-2509\(88\)85051-6](https://doi.org/10.1016/0009-2509(88)85051-6)

- [12] H. Alsmeyer, G. Albrecht, L. Meyer, W. Häfner, C. Journeau, M. Fischer, S. Hellman, M. Eddi, H.-J. Allelein, M. Bürger, B.R. Sehgal, M. K.Koch, Z. Alkan, J.B. Petrov, M. Gaune-Escard, E. Altstadt, G.Bandini, Ex-vessel core melt stabilization research (ECOSTAR), Nuclear Engineering & Design, Volume 235, pp 271–284, 2005, <https://doi:10.1016/j.nucengdes.2004.08.040>
- [13] J. Zhou, H. L. Tsai and T. Lehnhoff, Investigation of transport phenomena and defect formation in pulsed laser keyhole welding of zinc-coated steels, Journal of Physics D: Applied Physics, vol. 39, pp. 5338-5355, 2006. <http://stacks.iop.org/JPhysD/39/5338>
- [14] Harding, J.H., Martin, D.G, Potter, P.E. (1989). Thermophysical and thermochemical properties of fast reactor materials (EUR--12402). Commission of the European Communities (CEC)
- [15] S. Sitharamayya and K. S. Raju, Heat transfer between an axisymmetric jet and a plate held normal to the flow, The Canadian Journal of Chemical Engineering, vol. 47, pp. 365–368, Aug. 1969. <https://doi.org/10.1002/cjce.5450470412>
- [16] A. Lecoanet, F. Payot, C. Journeau, N. Rimbert, M. Gradeck, Study of the ablation consecutive to jet impingement on a meltable solid – Application to SFR core-catcher, Nuclear Engineering and Design 377 (2021) 111147, <https://doi.org/10.1016/j.nucengdes.2021.111147>

### Fig. Captions List

- Fig. 1 (Left) Schematic cross-section of a pool-type SFR with discharge tubes and a core-catcher. (Right) ASTRID cross-section
- Fig. 2 Possible ablative outcomes at impact of a free corium jet on a core-catcher.
- Fig. 3 schematic view of the ablation and associated quantities, from [6].
- Fig. 4 HANSOLO experimental facility. TT: Temperature Transducer; PT: Pressure Transducer; LT: Level Transducer; TC: Thermocouple.
- Fig. 5 Preparation of the transparent ice block before the test
- Fig. 6 Schematic of JIMEC test facility
- Fig. 7 Picture of JIMEC 2 test set-up
- Fig. 8 (a) front view of the test substrate in upside down position ; (b) location of the thermocouples
- Fig. 9 evolution of the shape before ( $t^*=-0,5$ ), at the transition ( $t^*=0$ ) and after ( $t^*=-0,5$ );  $T_j = 30\text{ }^{\circ}\text{C}$
- Fig. 10 pictures of JIMEC1, (a) flowing film regime, (b) pool regime
- Fig. 11 comparison of the normalized depths as a function of time
- Fig. 12 a) cut of JIMEC-1 ; b) Cut of JIMEC-2 ; c) Comparison of measured post-test contour of JIMEC-1 and JIMEC-2
- Fig. 13 comparison of HANSoLO results with existing scaling laws



**Table Caption List**

Table 1	Summary of experimental conditions available with HAnSoLO
Table 2	Composition of stainless steel 1.4301 according to DIN EN 10088-3.
Table 3	Material properties of metallic melt at 2050 °C and test substrate.
Table 4a	Details of the experiments performed with HAnSoLO
Table 4b	Uncertainties of the experiments performed with HAnSoLO
Table 5	Details of JIMEC 1 and JIMEC 2

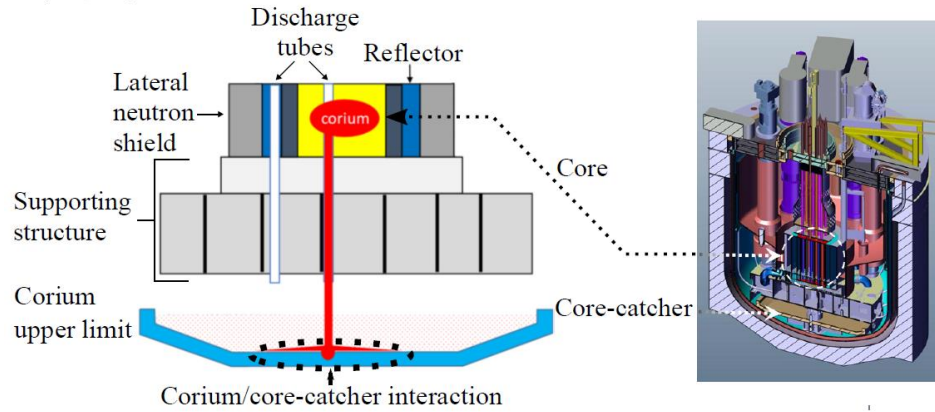


Fig. 1: (Left) Schematic cross-section of a pool-type SFR with discharge tubes and a core-catcher. (Right) ASTRID cross-section

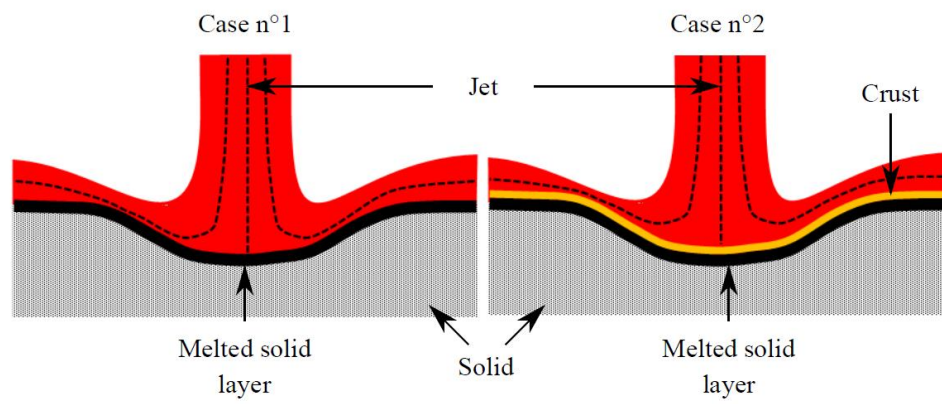


Fig. 2: Possible ablative outcomes at impact of a free corium jet on a core-catcher

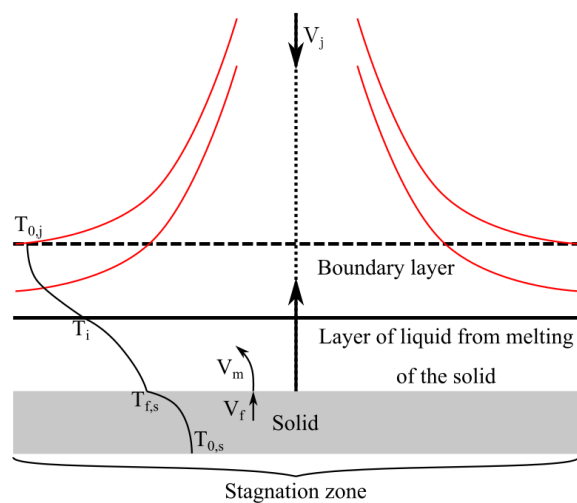


Fig. 3: schematic view of the ablation and associated quantities, from [6].

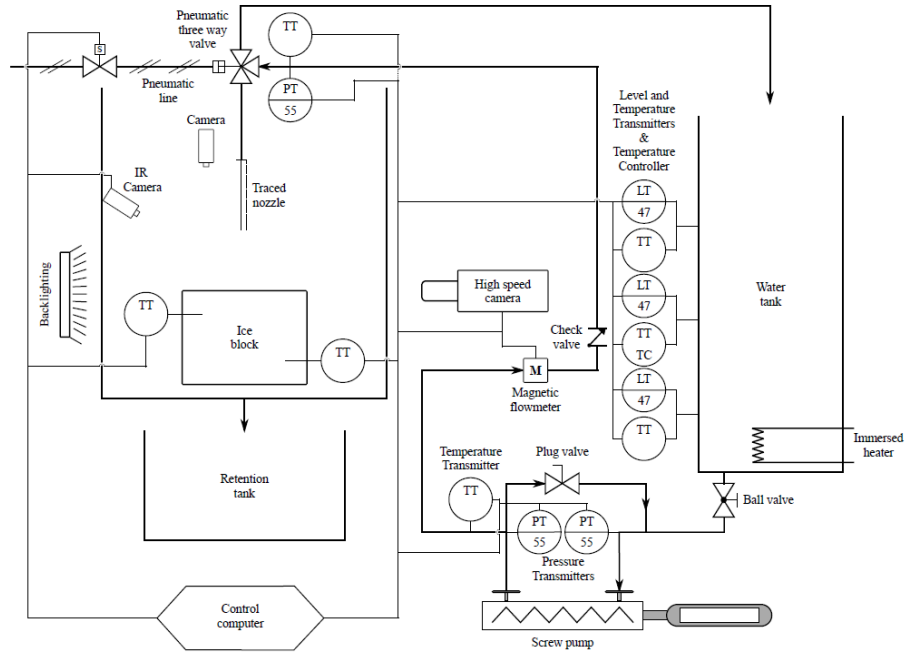


Fig. 4: HANSOLO experimental facility. TT: Temperature Transducer; PT: Pressure Transducer; LT: Level Transducer; TC: Thermocouple.

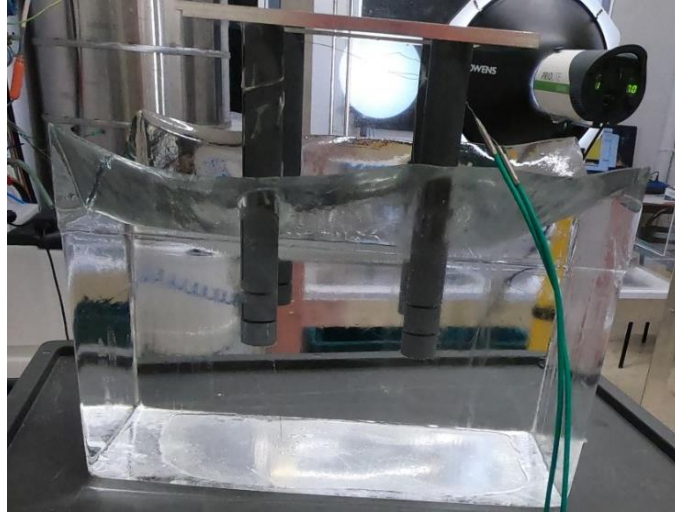


Fig. 5: Preparation of the transparent ice block before the test

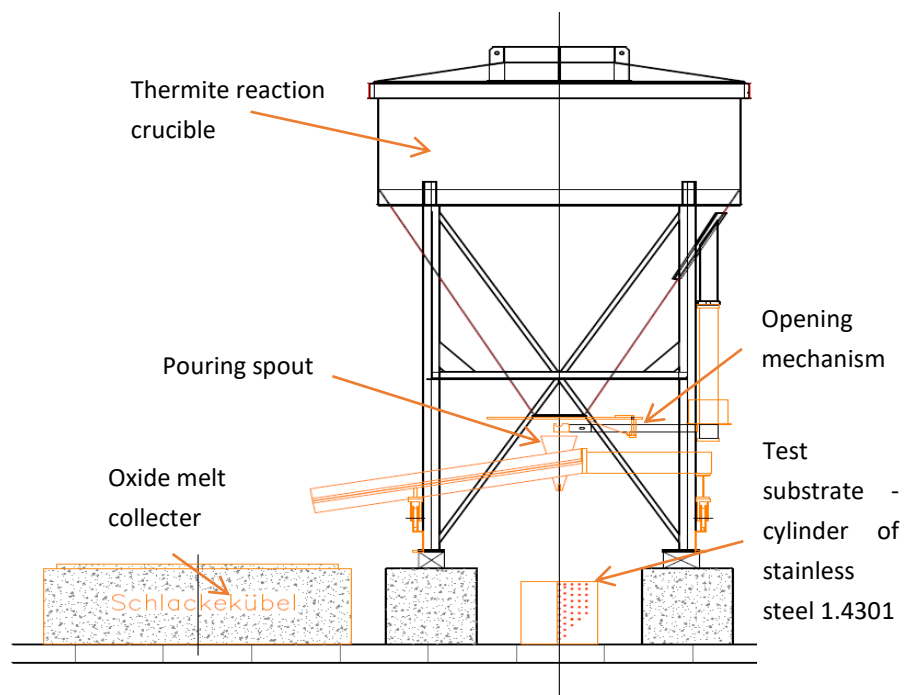


Fig. 6: Schematic of JIMEC test facility



Fig. 7: Picture of JIMEC 2 test set-up



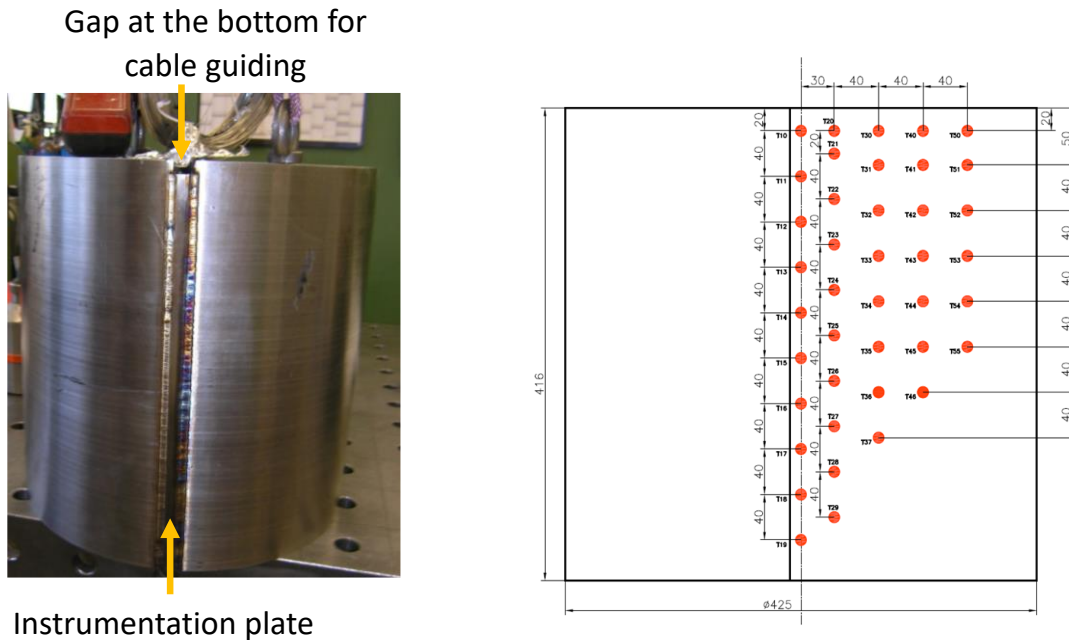


Fig. 8 : (a) front view of the test substrate in upside down position ; (b) location of the thermocouples

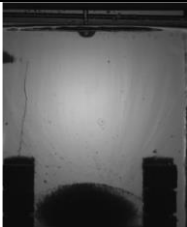
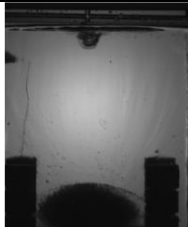
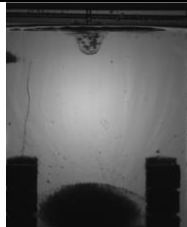
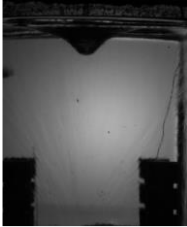

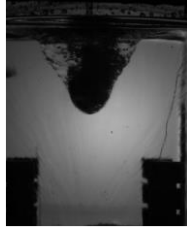
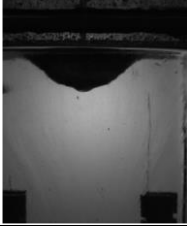

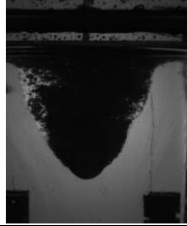
$(t-t_{pe})/t_{pe}$ Ref.	0,5	1	1,5
611			
613			
615			

Fig. 9: evolution of the shape before ( $(t-t_{pe})/t_{pe} = 0.5$ ), at the transition ( $(t-t_{pe})/t_{pe} = 1$ ) and after ( $(t-t_{pe})/t_{pe} = 1.5$ );  $T_j = 30\text{ }^{\circ}\text{C}$ . Nozzle diameter 6 mm. Jet velocity: 1.5 m/s for 611, 5.1 m/s for 613 and 10.2 for 615.

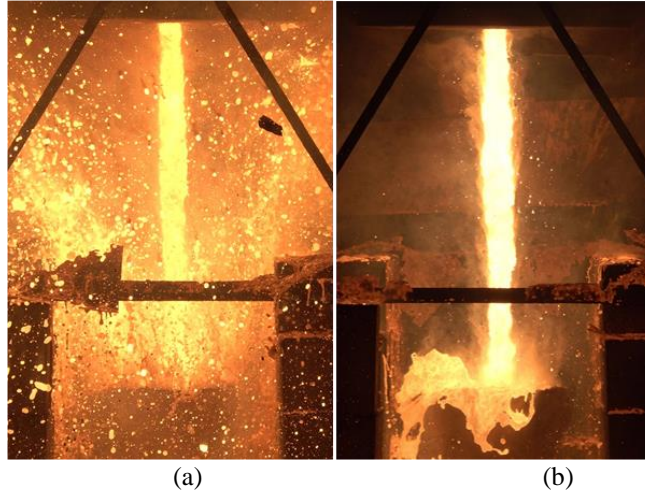


Fig. 10: pictures of JIMEC1, (a) flowing film regime, (b) pool regime

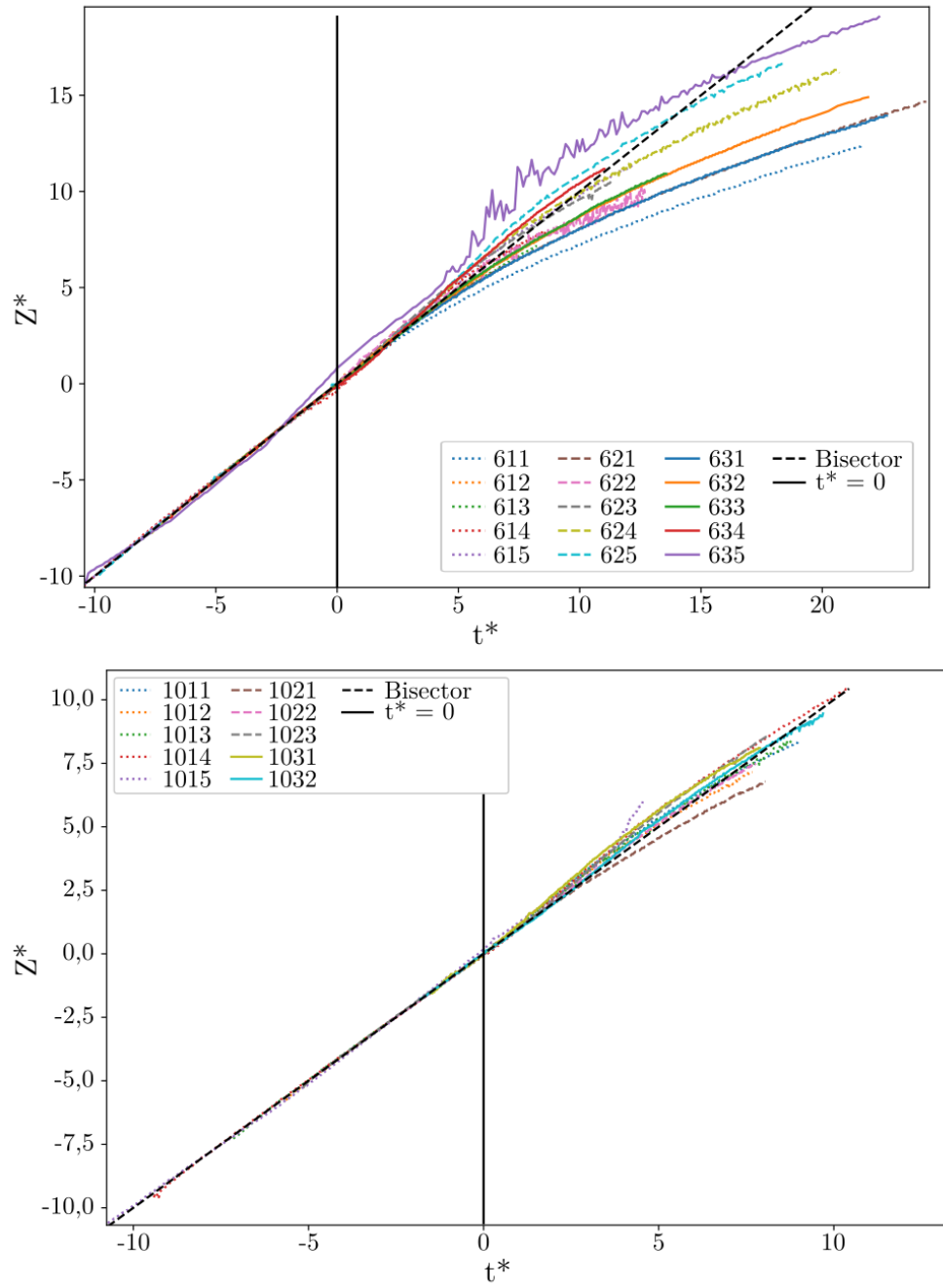


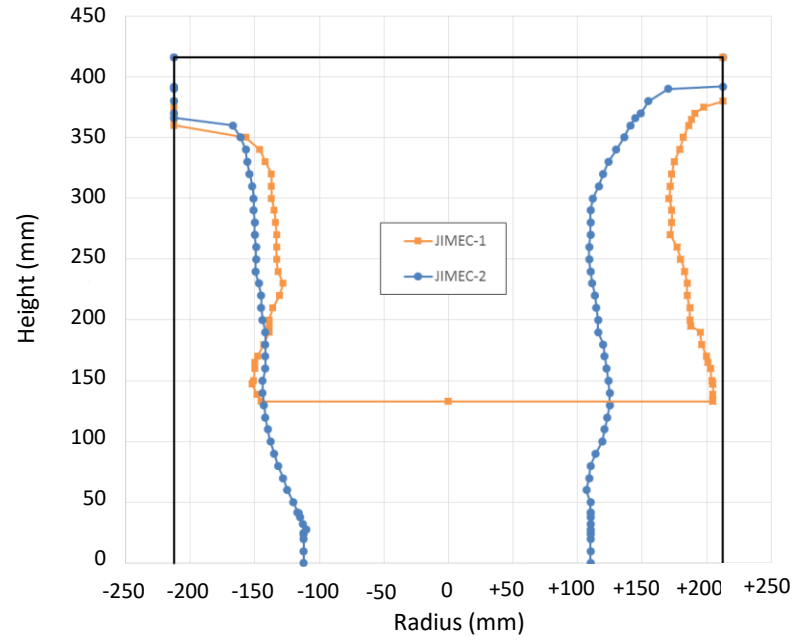
Fig. 11: comparison of the normalized depths as a function of time details of the experiments performed are given in Table 4a



(a)



(b)



(c)

Fig. 12: Post-test analysis of the substrates in JIMEC experiments: a) Cut of JIMEC-1 substrate; b) Cut of JIMEC-2 substrate ; c) Ablation Contours of JIMEC-1 and JIMEC-2 substrates

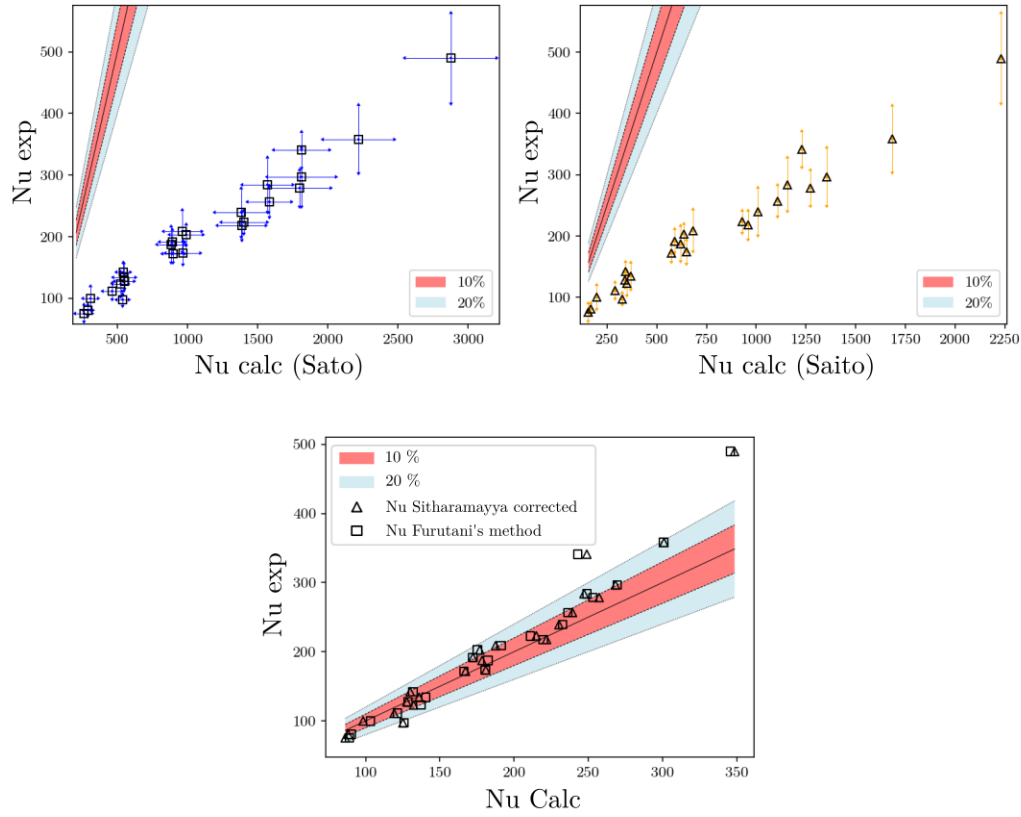


Fig. 13: comparison of HANSoLO results with existing scaling laws. Top: parity plots showing the evolution of the experimental Nusselt number as a function of the Nusselt number computed using the scaling law of Sato et al. [4] and the one reported by Saito et al. [1]. Bottom: parity plot showing the evolution of the experimental Nusselt number as a function of the Nusselt number computed using the scaling law of Sitharamayya et al. [15] as per recommended by Swedish et al. [7] and the one computed using the method of Furutani et al. [5]. Are also represented the bisector and the 10 % and 20 % deviation from the bisector zones in respectively red and blue.

	Minimum	Maximum
Jet speed (m/s)	1	10
Jet's temperature	Ambient	80 °C
Nozzle's diameter (mm)	3	10
Reynolds number	4 000	270 000
Prandtl number	2.5	7.0

Table 1: Summary of experimental conditions available with HANSOLO

<b>Fe</b>	<b>Cr</b>	<b>Ni</b>	<b>Si</b>	<b>Mn</b>	<b>Mo</b>	<b>Al</b>
67-72	17.5-19.5	8.0-10.5	≤ 1.0	≤2.0		

Table 2: Composition of stainless steel 1.4301 according to DIN EN 10088-3.



	Density [kg/m <sup>3</sup> ]	viscosity [Pa s]	Thermal conductivity [W/m K]	Heat capacity [J/kg K]	Thermal diffusivity [m <sup>2</sup> /s]	Thermal expansion [1/K]
Metallic melt at 2050 °C	6400 [10,11]	0.001919 [11]	3.22 [11]	750	6.2957×10 <sup>-6</sup>	1.31×10 <sup>-4</sup> [11]
Test substrate at 20 °C	7900	-	15	500	-	1.6×10 <sup>-5</sup>

Table 3: Material properties of metallic melt at 2020 °C and test substrate

Ref.	$T_j$ (°C)	$V_j$ (m/s)	$D_j$ (mm)	$H$ (mm)	$Re \times 10^3$	Pr	B	We	Fr
611	30	1.5	5	5.8	11	5.42	0.37	185	6.7
612	30	2.8	5.8	6	21	5.30	0.38	646	11.7
613	30	5.1	6.0	6.5	39	5.37	0.38	2 199	21.2
614	30	7.6	6.0	6.5	57	5.36	0.38	4 823	31.3
615	30	10.2	6.0	6.8	77	5.35	0.38	8 663	42.0
621	48	1.2	4.9	4.3	13	3.70	0.60	131	5.6
622	49	2.3	5.6	6.0	24	3.64	0.61	456	9.7
623	50	5.1	5.9	6.0	55	3.55	0.63	2 274	21.2
624	50	7.5	6.0	6.1	82	3.55	0.63	4 963	31.2
625	51	10	6.0	6.0	109	3.53	0.63	8 769	41.4
631	67	1.4	4.8	5.8	19	2.67	0.84	170	6.4
632	65	2.8	5.8	5.5	37	2.77	0.81	682	11.6
633	69	5.2	5.9	5.0	74	2.60	0.87	2 462	21.6
634	71	7.6	6.0	6.0	112	2.52	0.89	5 282	31.5
635	71	10.1	6.0	5.0	147	2.54	0.88	9 225	41.5
1011	30	1.6	8.1	7.3	19	5.38	0.38	347	5.6
1012	31	2.8	9.4	8.8	35	5.31	0.38	1 095	9.2
1013	30	5.2	9.8	8.0	65	5.37	0.38	3 792	16.8
1014	30	7.6	9.9	8.6	95	5.35	0.38	8 065	24.3
1015	31	10.1	10.0	8.2	128	5.30	0.39	14 188	32.2
1021	50	1.6	7.9	8.3	29	3.56	0.63	385	5.85
1022	51	2.8	9.4	8.6	51	3.48	0.64	1 140	9.2
1023	50	5.2	9.8	9.4	94	3.56	0.63	3 970	16.8
1031	68	1.6	7.7	8.4	38	2.65	0.85	388	5.8
1032	70	2.8	9.4	8.4	68	2.57	0.87	1 200	9.3

Table 4a: details of the experiments performed with HAnSoLO

Ref.	$\Delta V_j$ (m/s)	$\Delta D_j$ ( $\mu\text{m}$ )	$\Delta \text{Re} \times 10^3$	$\Delta \text{Pr}$	$\Delta B$	$\Delta \text{We}$	$\Delta \text{Fr}$
611	0,1	170	1,3	0,29	0,03	26	0,5
612	0,12	91	2,0	0,29	0,03	65	0,6
613	0,20	96	3,7	0,29	0,03	217	1,0
614	0,29	98	5,5	0,29	0,03	469	1,5
615	0,37	99	7,3	0,29	0,03	829	1,9
621	0,14	37	2,4	0,16	0,04	34	0,9
622	0,13	100	2,5	0,16	0,04	60	0,7
623	0,23	97	5,2	0,16	0,04	252	1,1
624	0,32	98	7,6	0,16	0,04	533	1,6
625	0,40	99	9,9	0,15	0,04	898	2,0
631	0,06	120	1,4	0,10	0,04	15	0,3
632	0,12	94	3,2	0,11	0,04	75	0,6
633	0,23	98	6,7	0,10	0,04	278	1,2
634	0,34	99	10	0,09	0,04	594	1,7
635	0,38	99	12	0,09	0,04	913	1,9
1011	0,03	80	1,1	0,29	0,03	14	0,1
1012	0,06	85	2,4	0,28	0,03	58	0,2
1013	0,11	95	7,8	0,29	0,03	218	0,5
1014	0,17	98	7,1	0,29	0,03	475	0,7
1015	0,23	99	9,5	0,28	0,03	847	0,9
1021	0,03	76	1,4	0,16	0,04	15	0,1
1022	0,06	86	3,1	0,15	0,04	62	0,2
1023	0,11	94	6,0	0,16	0,04	229	0,4
1031	0,03	80	1,6	0,10	0,04	15	0,1
1032	0,06	87	3,8	0,10	0,04	68	0,3

Table 4b: Uncertainties of the experiments performed with HAnSoLO

	H (mm)	D0 (mm)	Vj,0 (m/s)
JIMEC 1	1080	37	4,7
JIMEC 2	940	24	5

Table 5: Details of JIMEC 1 and JIMEC 2